Shunt Active Parallel Filter, Grid Photovoltaic System

ACHWAK ALAZRAG, MOHAMED HAJJEJ, LASSAD SBIT[1]
Process Laboratory, Energetic, Environment and Electrical System (PEESE),
National Engineering School of Gabes (ENIG), University of Gabes,
TUNISIA

Abstract: - This paper introduces a study focused on managing a photovoltaic system connected to the electrical grid. The primary components of this system include solar arrays linked via a DC bus to an inverter situated on the grid side. Fluctuations in solar irradiance and temperature are swift, prompting the integration of maximum power point tracking (MPPT) within the inverter's control mechanism. The energy produced by the photovoltaic system is fed into the grid. This transfer is achieved through a proficient DC/AC conversion process, wherein the MPPT is integrated into the inverter's operation to regulate the levels of active and reactive power injected into the grid. The paper also delves into the employment of the Space Vector Modulation (SVM) control technique for the DC-AC inverter. It covers the implementation of a Shunt Active Power Filter (SAPF) with a three-phase four-wire configuration, consisting of four legs and adopting a split capacitor topology. Furthermore, the paper includes an exploration of the instantaneous power theory and the utilization of hysteresis block control for the SAPF. The findings of this study are demonstrated and analyzed using Matlab/Simulink software.

Key-Words: - Photovoltaic system, Boost converter, Bidirectional DC-DC converters, MPPT, SAPF, PWM.

Received: April 4, 2023. Revised: October 21, 2023. Accepted: November 12, 2023. Published: December 31, 2023.

1 Introduction

Photovoltaic energy has emerged as an intriguing and increasingly pertinent solution within the realm of electrical applications. This heightened interest can be attributed to the fact that photovoltaic energy sources are not only renewable but also widely accessible in various geographic locations. However, a significant drawback associated with photovoltaic power generation is its susceptibility to external factors, particularly fluctuations in solar radiation and temperature. This variability leads to an inherent instability in the generated power output. To circumvent this challenge and unlock the full potential of photovoltaic systems, the imperative to accurately track and maintain the maximum power point (MPP) of the photovoltaic generator becomes evident. At the core of this endeavor lies the concept of the maximum power point (MPP), which represents the singular operating state at which the photovoltaic generator yields the highest possible power output for a given load. Consequently, to optimize the overall efficiency of a photovoltaic system, it is paramount to devise methodologies for continuously identifying and maintaining this optimal MPP.

In the pursuit of achieving this objective, various algorithms and techniques have been developed for what is known as Maximum PowerPoint Tracking (MPPT). These algorithms seek to dynamically adjust the operational parameters of the photovoltaic system, such as the duty cycle of a DC/DC converter or other control variables, to constantly align the system's operating point with the elusive MPP. One such technique is the fuzzy logic controller (FLC), which operates by processing inputs such as error signals and their variations to determine the appropriate adjustments needed to approach the MPP.

This research paper delves into a comprehensive exploration of a grid-connected photovoltaic system. The central focus of this study is the integration of MPPT control mechanisms into the inverter control system. By seamlessly incorporating MPPT algorithms within the inverter's operation, the study aims to ensure that the active and reactive power levels injected into the grid are optimized in response to changing environmental conditions. This dynamic control mechanism ultimately enhances the energy-harvesting efficiency of the photovoltaic system.

Within the scope of this study, the use of hysteresis current control (RCe) is adopted, representing a relatively simple yet effective method for regulating the system. However, it is acknowledged that this approach has its limitations, particularly in terms of variable switching frequency, [1]. To mitigate these limitations and refine the control mechanism, the paper introduces a modulated hysteresis control strategy, [2]. This innovation involves overlaying a triangular signal with the desired switching frequency onto the reference current signal, thereby facilitating a more precise and controlled system response. Furthermore, the research introduces a Shunt Active Power Filter (SAPF) that operates in parallel with the load side. The SAPF is designed to address the presence of high-order harmonic currents within the load, enhancing power quality and mitigating potential disruptions caused by harmonic distortions. The widespread use of nonlinear loads in industrial, commercial, and residential systems has led to significant power quality issues in contemporary power distribution systems. Among these issues, harmonic currents and reactive power stand out as major concerns. Shunt Active Power Filters (SAPFs) have emerged as the most commonly employed solution for managing harmonic currents, compensating for reactive power, and addressing neutral current issues in distribution systems. Typically, these systems are connected at the Point of Common Coupling (PCC), which is the point of connection between nonlinear loads and the electrical grid. The block diagram of the SAPF is depicted in Figure 1, [1]. Unlike passive power filters (PPFs), which mainly consist of inductive and capacitive elements (L-C) and provide fixed compensation, SAPFs offer dynamic and adaptable solutions. They can actively respond to power quality problems, delivering precise control while minimizing the resonance effects often associated with passive filters. SAPFs also offer advantages in terms of sizing and flexibility, making them the preferred choice for tackling power quality challenges, [3].

Presently, researchers and developers are primarily concentrating on enhancing both the design and control aspects of SAPFs (Static Active Power Filters) for three-phase four-wire (3ph-4W) nonlinear loads, [4]. Various SAPF topologies have emerged to address these challenges, including the four-leg (4L) configuration, [5], as mentioned in Figure 2, the split capacitor or two capacitors (2C) approach, [6], presented in Figure 3, and the three H-bridges (3-HB) topology (Figure 4), with each H-bridge consisting of four switches arranged in an H shape, [7].

In the split capacitor topology, the neutral wire is positioned between two capacitors, necessitating an additional control loop to maintain balance in DC voltages between the capacitors. Conversely, the 4L configuration introduces two active switches to the fourth leg (neutral wire) to balance the neutral current, resulting in superior performance compared to the 2C topology. This configuration has been extensively explored in various research studies, [8], [9]. In contrast, the 3-HB inverter topology employs three full H-bridges with a shared DC-link capacitor, requiring three single-phase isolated transformers to connect the 3-HB filter to the system and more switches than other configurations, [10].

While some researchers have focused on optimizing and creating various parallel active filter topologies, [11], others have delved into perfecting the control aspect of these filters, which represents their "heart." The filtering efficiency is closely tied to the effectiveness of the reference current extraction algorithm. These methodologies generally fall into two main categories: frequency domain methods and time domain methods.

In the frequency domain approach, techniques like the fast Fourier transform (FFT) are utilized to extract harmonic components from distorted voltage and current signals, [12]. Despite their ability to provide precise values of harmonic amplitude and phases, these techniques have drawbacks, such as aliasing effects and spectral leakage, [13]. Additionally, they suffer from slow response times due to the substantial computational load imposed by FFT calculations, necessitating complex and costly systems to operate the filter in real time.

This has led other researchers to focus on time domain methods, which include the p-q theory, [14], instantaneous reactive power theory, [15], synchronous reference frame theory (SRF), [16] and p-q-r theory, [17], [18]. Among these, the SRF technique stands out for its use of a phase-locked loop (PLL) system, ensuring undistorted transformation angles even under unbalanced source conditions. Consequently, SRF can be employed for both voltage and current reference generation, with the reference currents serving as inputs to the power switch control block.

Hysteresis control algorithms (HCA) are considered simple and practical techniques for SAPF and power switch device control. HCA operates with two predefined bands, ensuring that the modulated currents remain within these specified limits. This leads to the compensating current closely tracking the reference current. HCA determines the duration of the VSI (Voltage Source Inverter) switches' "ON" and "OFF" states, resulting in straightforward implementation, robustness, and high performance, [19], [20]. However, HCA has its limitations, including a limited frequency range and nonlinear effects, [2]. To address these issues, researchers have introduced a new technique called pulse width modulation (PWM) control, which produces a modulation signal to adjust the duty cycle of power electronic switches, [21].

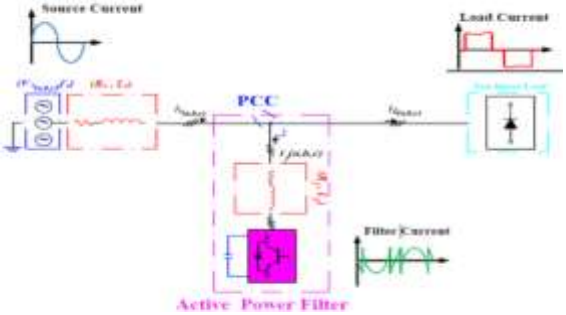

Fig. 1: Bloc diagram of the SAPF connected to the distribution network

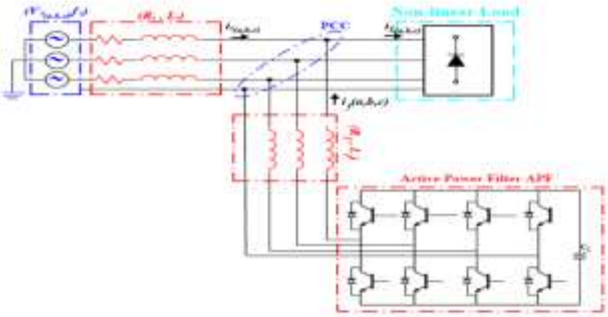

Fig. 2: Bloc diagram of the SAPF connected to a distribution network with four legs topologies

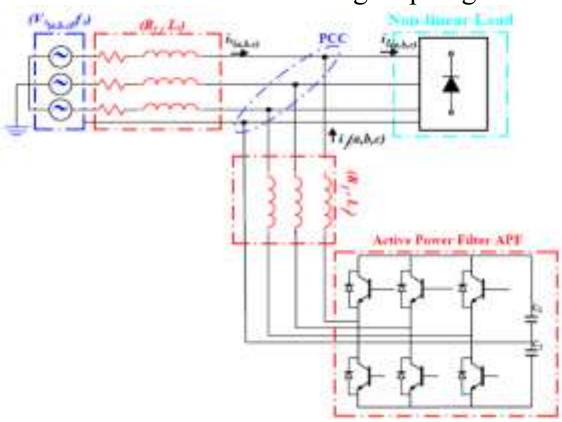

Fig. 3: Bloc diagram of the SAPF connected to the distribution network with four legs and mid-point capacitor topologies

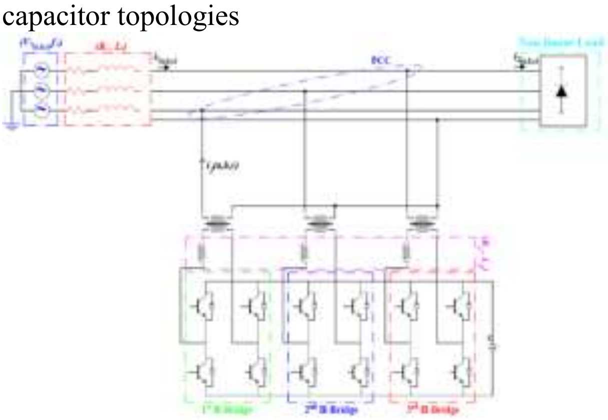

Fig. 4: Bloc diagram of the SAPF connected to the distribution network with 3 half bridge topologies.

This study introduces a control system designed for a photovoltaic (PV) system connected to the electrical grid. The primary system components consist of solar arrays connected to an inverter via a DC bus. To effectively handle the rapid fluctuations in solar irradiance and temperature, the control system incorporates a technique known as maximum power point tracking (MPPT) into the inverter's operation. The goal is to ensure that the PV generator operates at its maximum power point (MPP), which corresponds to the point of the highest power output.

There are various algorithms available for MPPT, [22], [23] and in this research, we have employed the Perturb & Observe (P&O) method, [24]. The P&O algorithm takes an error signal as input and produces the duty ratio of the DC/DC converter (or its variation) as output, aiding in the discovery of the MPP. This configuration enhances the system's versatility and efficiency by enabling energy storage and supply as needed.

To address high harmonic currents in the electrical grid, a SAPF (Static Active Power Filter) is connected in parallel on the grid side for compensation (Figure 5). The overall effectiveness of the APF depends on the efficiency of both the reference current extraction technique and the control of VSI switching devices. For reference current extraction, a mathematical algorithm based on the SRF technique was developed and implemented. This algorithm allowed for the real-time extraction of harmonics generated by CFLs from the power source. These currents were sensed using four sensors placed on the load side. Additionally, the SRF technique utilized the PLL block to provide the fundamental frequency for synchronization purposes. The compensation currents were then compared to the actual current provided by the VSI at the PCC. Any discrepancies were used as error currents and applied to the HCA to generate switching signals for the VSI based on IGBT switches. It's important to note that while HCA offers numerous advantages, it is susceptible to chattering, resulting in variable switching frequencies, which remain unresolved. To address this concern, a Pulse Width Modulation (PWM) controller was integrated into the system instead of HCA. This PWM controller stabilized the switching frequency and mitigated associated harmonic losses.
The paper is structured as follows: Section 2 elaborates on the Photovoltaic Generator (PVG) and the algorithms used for MPPT. In Section 3, the Space Vector Modulation (SVM) control technique for the DC-AC inverter is thoroughly examined. The

intricacies of a three-phase four-wire Shunt Active Power Filter (SAPF) with a four-leg configuration and split capacitor topology are presented in Section 4. Additionally, this section provides an overview of the Synchronous reference frame theory to calculate the compensation current and the Fixed hysteresis block control applied to control the switching device of the voltage source inverter (VSI). Moving forward, Section 5 provides a detailed analysis of simulation results and the efficacy of harmonic mitigation strategies. Finally, Section 6 concludes the paper by summarizing the findings and contributions of this research endeavor.

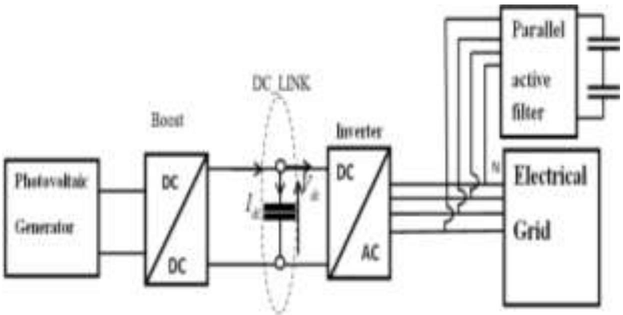

Fig. 5: Photovoltaic system connected to electrical grid with active parallel filter

2 PV Array

Photovoltaic devices are nonlinear devices. Their parameters are sunlight and temperature-dependent. Sunlight is converted into electricity by photovoltaic cells. Photovoltaic arrays consist of parallel and series of PV modules. To form the panels or modules cells are grouped. Not only a DC load can be fed by the voltage and current produced at the terminals of a PV but they can also be connected to an inverter to produce alternating current. Photovoltaic cell models have been used for the description of photovoltaic cell behaviors for researchers and professionals for a long time. The Single diode circuit model is among the most common models that are used to predict energy production in PV cells.

A PV module is formed by assembling several photovoltaic cells, which can be connected in series and/or in parallel. This configuration allows obtaining specific electrical characteristics according to the needs of the system. By grouping several photovoltaic modules, whether in series, in parallel, or both, a larger photovoltaic field or generator is created. This combination of modules increases the power and solar energy production capacity to meet the requirements of the electrical load or the connected system.

2.1 Modeling of a PV Cell with a Diode

A PV solar cell is essentially a large surface PN electronic diode that, when exposed to light (photons), generates an electrical voltage (in volts). It operates similarly to a diode for cell polarization, allowing the unidirectional flow of electric current. Additionally, the solar cell includes two resistances, one in series and one in parallel (shunt), which are responsible for energy losses in the circuit. These resistances affect the overall efficiency of the solar cell by dissipating a portion of the produced energy. The one-diode model has been used in several research works related to the modeling of the PV system to obtain its characteristics. The equivalent electrical schematic of this model is illustrated in Figure 6.

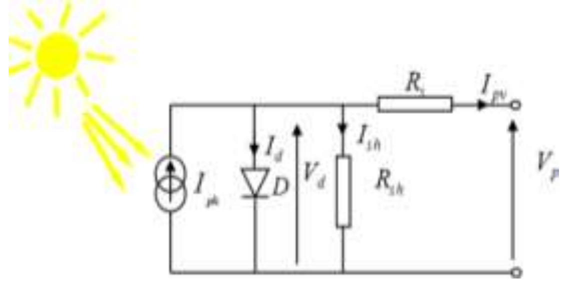

Fig. 6: Equivalent model of a real cell

The resistances R_s and R_{sh} are responsible for accounting for losses related to manufacturing defects; R_s represents various contact and connection resistances, while leakage currents due to the diode and edge effects of the junction are characterized by R_{sh} . The following relationship is expressed using Kirchhoff's current law:

$$I_{PV} = I_{ph} - I_d - I_{sh} \tag{1}$$

And

$$V_d = V_p + R_s.I_{PV} \tag{2}$$

With:

$$I_d = I_S \cdot \left\lfloor \exp\left(\frac{V_d}{V_T}\right) - 1 \right\rfloor \tag{3}$$

Photo-current of the module:

$$I_{PV} = I_{ph} - I_S \cdot \left[\exp\left(\frac{V_{PV} + R_S.I_P}{V_T}\right) - 1 \right] - \frac{V_{PV} + R_S.I_{PV}}{R_{sh}} \tag{4}$$

I_{ph}: photo-current.

I_{cc}: Short circuit current of the cell under the standard conditions reference (E_{ref} and T_{ref}).

E: Sunshine received by the cell (W/m^2).

E_{ref} : Reference sunshine.
K_{icc}: Current short-circuit-temperature coefficient (A/C).

$$V_T = \frac{n.K_B.T_j}{q}) \tag{5}$$

Where:
I_s: Inverse current saturation of the diode.
q: Charge of an electron.
K_B: Constant of Boltzmann.
T_j: temperature of the junction(C).
n: Ideal factor of the solar cell.
I_{PV}: the output current of the photovoltaic cell.
V_{PV}: the output voltage of the photovoltaic cell.

2.2 PV Generator

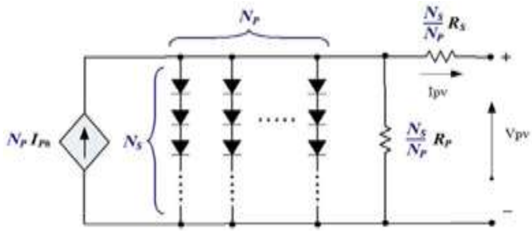

Fig. 7: PV generator

As shown in the Figure 7 the PV panels consisting of n_s cells connected in series (the same current flows through the cells, and the resulting characteristic of the series arrangement is obtained by adding the voltages at a given current, i.e., the voltages add up, and the current remains constant) and n_p cells connected in parallel (the cells are subjected to the same voltage, and the characteristic resulting from the grouping is obtained by adding the currents at a given voltage: the currents add up, and the voltage remains constant).

The total current delivered by the PV array, I_{pvg} is described by:

$$I_{pvg} = n_p.I_{ph} - n_p I_S.\left[\exp(\frac{V_{PV}+R_S.I_P}{n_s V_T})-1\right] - \frac{V_{PV}+R_S.I_P}{R_{sh}} \tag{6}$$

Incorporating series resistance and shunt resistances provides an accurate modeling opportunity for the PV cell. Rs corresponds to internal losses due to current flow, and Rsh corresponds to the leakage current to the ground. The incorporation of series modules (cells) ns increases the output voltage of the photovoltaic array, and the incorporation of parallel modules np increases the output current of the photovoltaic array.

Manufacturers of PV modules provide reference values for specified operating conditions, such as STC (Standard Test Conditions), where the irradiance is 1000 Wm-2, and the cell temperature is 25°C. Practical operating conditions often differ from the desired standard conditions, and mismatch effects can also impact the real values of these mean parameters.

The simulation was carried out for different levels of irradiance and also for different temperature levels. Irradiation levels were varied from 0 W/m² to 1000 W/m², and the resultant P-V and I-V curves can be seen in Figure 8 and Figure 9.

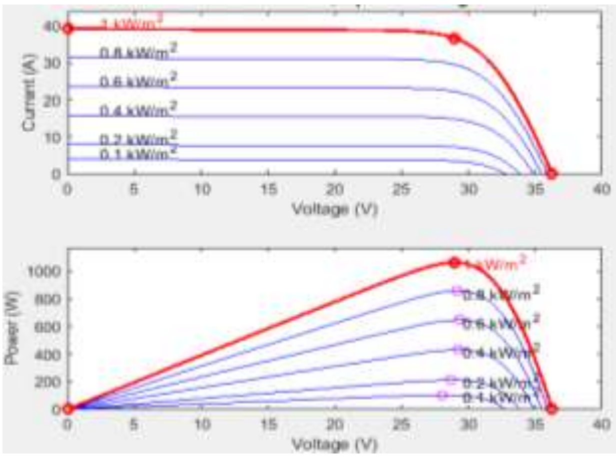

Fig. 8: V-I and P-V Characteristics of PV module at different irradiation

Temperature was varied from 25C to 75C and the resultant P-V and I-V curves can be seen in Figure 9.

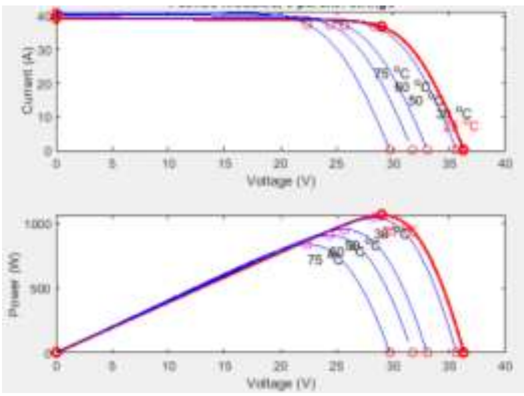

Fig. 9: V-I and P-V Characteristics of PV module at different temperatures

The simulation results obtained from Figure 8 and Figure 9 shows that the voltage variation with changes in irradiation is minimal, whereas, with an increase in temperature, the voltage decreases.

Typically, the voltage will decrease. It can also be observed that each curve has an operating point for a certain operating voltage at which the module produces the maximum power. This point is known as the Maximum Power Point (MPP). The goal is to operate the photovoltaic system always at this maximum point to extract maximum power from the module.

Additionally, it can be observed that at different levels of solar irradiation, the open circuit voltages are almost the same, and at different levels of temperatures, the short circuit currents are almost the same. This, in turn, illustrates that at different levels of solar irradiation, the voltage at which the maximum power point is located is almost the same. However, at different levels of temperatures, the maximum power point is located at various operating voltages that are far from each other. This maximum power point varies at every instance, and to have an efficient system, it is necessary to track this maximum point at every instance of operation.

2.3 Efficiency of a Photovoltaic Generator

The efficiency of a cell is the ratio between the available maximum power and the power of the incident radiation; it is given by :

$$\eta = \frac{P_{pm}}{P_{in}} = \frac{I_m . V_m}{A . E_a} \tag{7}$$

P_{in}: Incident power on the surface of the photovoltaic cell (W),
E_a : Incident global illumination on the photovoltaic cell (W/m^2),
A: Total surface area of the photovoltaic cell (m^2).

2.4 Fill Factor

Used to assess the quality of a photovoltaic cell, it is defined as the ratio between the point of maximum power and the power at the short-circuit current and open-circuit voltage.

$$FF = \frac{P_{pm}}{V_{co} . I_{cc}} = \frac{\eta . A . E_a}{V_{co} . I_{cc}} \tag{8}$$

3 Maximum Power Point Tracking

The maximum power (MP) is obtained when the solar panel is operated at the voltage where the global maximum of the P-V characteristic lies. It shows that for one specific operating point, the maximum power output can be obtained from the solar panel. This point on the P-V characteristic curve is called the Maximum Power Point (MPP). This point always lies on the knee of the I-V curve of the solar panel. In summary, it can be concluded that on the I-V curve of the solar panel, there is a point called MPP (Maximum Power Point), which always occurs on the knee of the curve where the generated PV power is maximized. This MPP changes with the change of irradiation and temperature [4]. The irradiation and temperature are dynamic; therefore, the MPP tracking algorithm has to work practically in real-time by updating the duty cycle constantly and thereby maintaining the speed and accuracy of tracking (Figure 10).

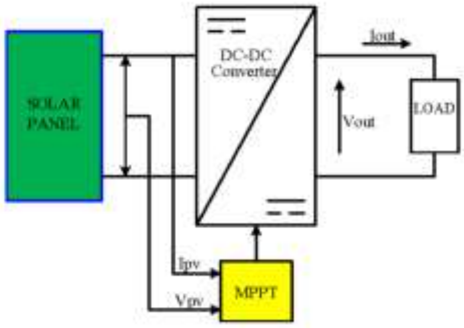

Fig. 10: MPPT Schematic Block Diagramm

The algorithm is executed by the MPPT controller to find the MPP. The measured output voltage and current of the solar panel are inputs of the controller. The algorithm performs its calculations depending on these inputs. The controller produces an output which is the adjusted duty cycle of the PWM. It drives the DC-DC converter’s switching device. For every different operating point, the controller produces a different duty cycle. To obtain the maximum power from the solar panels, an efficient tracker algorithm is required for the MPPT. The tracker algorithm’s task is to track the maximum power point of the solar panel as accurately as possible. The algorithm also has to be fast and reliable as well. There are several principles of operation of MPPT algorithms more or less successful based on the properties of the PV array. And Table 1 summarizes the main specifications of the various and famous MPPT algorithms previously presented. Was evaluated and compared these algorithms in terms of complexity, precision, speed, and technical knowledge of PV panel settings, [25], [26].

Table 1. Technical comparison of MPPT

MPPT	P&O	InC	LF
Sensor used	1 voltage 1 current	1 voltage 1 current	1 current
Identification pv panel parameters	Not necessary	Not necessary	Yes necessary
complexity	Low	Medium	High
Number of iterations	45	48	27
Speed of convergence	Medium	Medium	Very fast
Precision	95%	98%	99%

3.1 Perturb & Observe

The principle of this control algorithm is to generate disturbances by reducing or increasing the duty cyclic and observe the effect on the power output of the PV generator, [22], [27]. The P&O method operates periodically incrementing or decrementing the output terminal voltage of the PV and comparing the power obtained in the current cycle with the power of the previous cycle. If the voltage varies and the power increases, the control system changes the operating point in that direction, otherwise changes the operating point in the opposite direction. Once the direction for the change of current is known, the current is varied at a constant rate. This rate is a parameter that should be adjusted to allow the balance between faster response with less fluctuation in the steady state, [28]. The flowchart of this algorithm is presented in Figure 11.

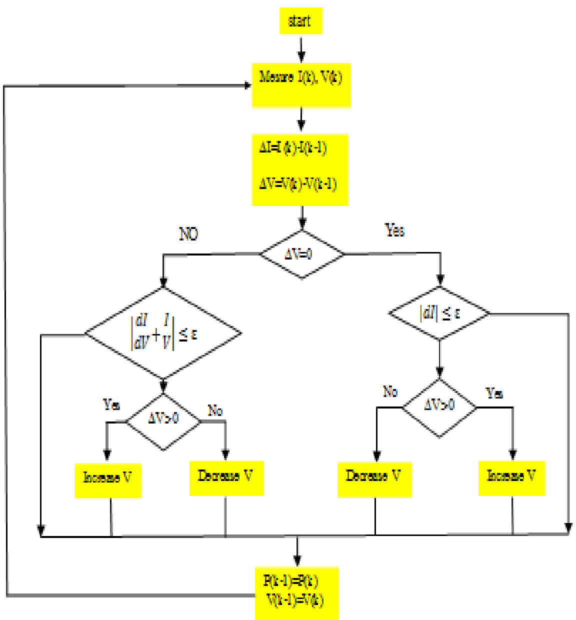

Fig. 11: Perturb and Observe algorithm

A modified version is obtained when the steps are changed according to the distance of the MPP, resulting in higher efficiency. A frequent trouble in P&O methods is that the output terminal voltage of the PV is perturbed every MPPT cycle even when the MPP is reached, resulting in loss of power.

3.2 Quadratic DC Bus Control

Due to the intermittent and fluctuating character of GPV, the voltage at the DC bus will be disturbed and fluctuating. This is why the DC bus voltage must be kept constant at its reference. In this case, the value of this voltage Vdc must be well chosen for proper operation of the PV system connected to the grid. The capacitor at the input of the inverter has two essential tasks:

a. In a steady state, it keeps the DC bus voltage constant with low oscillations.
b. it serves as an energy storage element to compensate for the difference in actual power between the load and the source during transient periods.

Figure 12 shows the DC bus voltage regulation loop to generate the reference power. The DC bus control generates the fluctuating power in the DC bus capacitor, subtracted from the power at the output of the inverter, which gives us the reference active power that must be fed into the grid. A dynamic reference of reactive power allows us for small powers to impose a zero reactive power. The DC power is:

$$P_{dc} = I_{dc}.V_{dc} \qquad 9$$

Then

$$P_{dc} = \frac{1}{2}.C_{dc}.\frac{dV_{dc}^{\;2}}{dt} \qquad 10$$

C_{dc}: the DC bus capacitor.
So,

$$V_{dc}(n) = \left[V_{dc}^{\;2}(n-1) + \frac{2T_e}{C_{dc}}(P(n) - P_{grid}(n)) \right]^{1/2} \qquad 11$$

T_e: Sampling period

The control strategy is divided into two blocks the first is for the calculation and the second is reserved for the control.

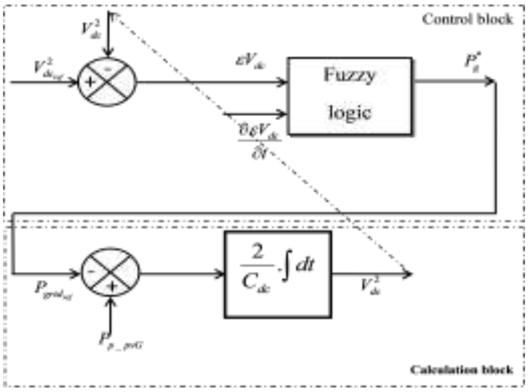

Fig. 12: Quadratic DC bus control

3.3 Three-phase Phase-Locked Loop (PLL) in the Park Area

The control of power converters requires, in the first phase, the reading of the electrical quantities of the electrical grid or possibly of the load and the reconstitution of reference quantities, currents, and voltages, to impose them on the regulators concerned. Under the conditions of unbalance of the network voltage system, we cannot under any circumstances guarantee synchronization of the phase θ_s used in the Park transform with that of the quantities of the network. As shown in the Figure 13 the PLL (Phase Locked Loop) technique is to reconstitute one of the components, direct or quadrature, of the fundamental voltage in the Park reference frame from a phase θ synchronized with the real phase θ of the grid voltage.

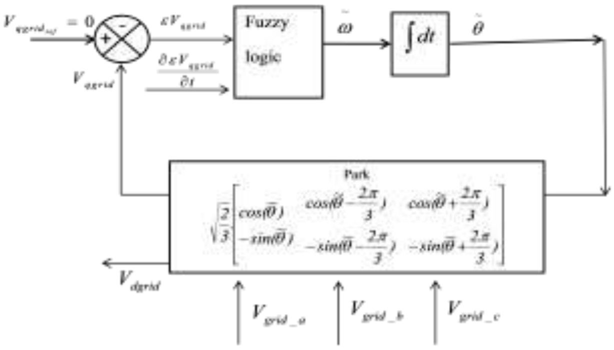

Fig. 13: PLL phase lock loop

The basic principle of the three-phase PLL in an unbalanced regime consists of applying an inverse Park transformation to the three-phase voltage system of the network and in slaving one of the components generated by this transformation, direct or quadrature, to zero by action on the network, angle of Park's frame of reference. The inputs of the PLL are the three-phase voltages of the electrical grid and the output is the detected phase angle. In the case of a balanced system, the three simple voltages of the grid are expressed as follows:

$$\begin{cases} V_{grid\_a} = \sqrt{2}.V_{grid}.\cos(\theta_v) \\ V_{grid\_b} = \sqrt{2}.V_{grid}.\cos(\theta_v - \frac{2\pi}{3}) \\ V_{grid\_c} = \sqrt{2}.V_{grid}.\cos(\theta_v + \frac{2\pi}{3}) \end{cases} \quad (12)$$

Where, V_{grid} is the rms value of the network voltage and $\theta_v = 2.\pi.f.t$ is the phase angle. By applying Park's transformation, the three previous tensions are rewritten in the graduation (d, q) as follows:

$$\begin{bmatrix} V_{dgrid} \\ V_{qgrid} \\ 0 \end{bmatrix} = P\theta \begin{bmatrix} V_{grid\_a} \\ V_{grid\_b} \\ V_{grid\_c} \end{bmatrix} \quad (13)$$

Or, $P\theta$ is the Park matrix. These leads:

$$\begin{bmatrix} V_{dgrid} \\ V_{qgrid} \\ 0 \end{bmatrix} = \sqrt{\frac{3}{2}} V_{grid} \begin{bmatrix} \cos(\theta-\theta_v) \\ -\sin(\theta-\theta_v) \end{bmatrix} \quad (14)$$

$$\begin{bmatrix} V_{dgrid} \\ V_{qgrid} \\ 0 \end{bmatrix} = \sqrt{\frac{3}{2}} V_{grid} \begin{bmatrix} \cos(\theta) & \cos(\theta-\frac{2\pi}{3}) & \cos(\theta+\frac{2\pi}{3}) \\ -\sin(\theta) & -\sin(\theta-\frac{2\pi}{3}) & -\sin(\theta+\frac{2\pi}{3}) \end{bmatrix} * \begin{bmatrix} \cos(\theta_v) \\ \cos(\theta_v - \frac{2\pi}{3}) \\ \cos(\theta_v + \frac{2\pi}{3}) \end{bmatrix} \quad (15)$$

By applying trigonometric relation, the previous equation is simplified as follows:

$$\begin{bmatrix} V_{dgrid} \\ V_{qgrid} \\ 0 \end{bmatrix} = \sqrt{\frac{3}{2}} V_{grid} \begin{bmatrix} \cos(\theta-\theta_v) \\ -\sin(\theta-\theta_v) \end{bmatrix} \quad (17)$$

The angle θ can be obtained by synchronizing the voltage vector along the d axis of the synchronous coordinates. We then estimate θ_v to be roughly equal to θ. This gives:

$$\sin(\theta-\theta_v) \approx \theta-\theta_v \quad (18)$$

A linear system is then obtained. Thus, the direct component V_{dr} is the image of the amplitude of the voltage measured and the component in quadrant V_{qr} is equal to zero and controlled by a fuzzy regulator.

Under the last hypothesis, the voltage V_{qr} can be expressed as follows:

$$V_{qr} \approx \sqrt{3} V_{grid} (\theta - \theta_v) \tag{19}$$

The currents I_{dr} and I_{qr} will respectively be a direct image of the active and reactive power. the linear model of the PLL is given in the Figure 14:

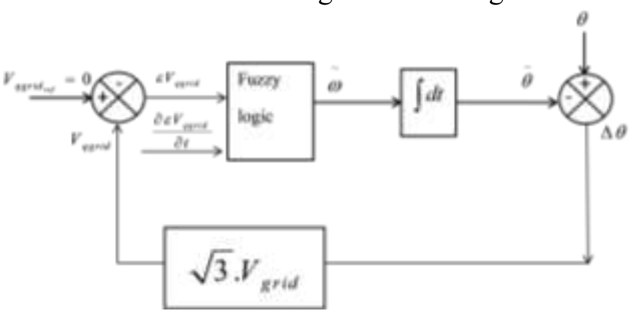

Fig. 14: Simplified diagram of the three-phase PLL

The integrated filter is of the low pass type, its purpose is to improve the quality of the signals exchanged between the Cr converter and the grid parameter connection (R_f, L_f). Its cut frequency f_c is given by relation (20):

$$f_c = \frac{R_f}{2\pi L_f} \tag{20}$$

By application of the Laplace transform, the currents at the filter output (R_f, L_f) will then be expressed as follows:

Numerically we write:

$$\begin{cases} I_{dgrid} = \dfrac{V_{dcr} - V_{dgrid} + \omega L_f I_{qgrid}}{R_f + pL_f} \\ I_{qgrid} = \dfrac{V_{qcr} - V_{qgrid} + \omega L_f I_{dgrid}}{R_f + pL_f} \end{cases} \tag{16}$$

4 Shunt Active Power Filter with Three Phases, Four Wires, Four Legs and a Split Capacitor Topology

In this study, a three-phase four-wire SAPF is developed, consisting of three legs/arms based on two stages with a midpoint capacitor topology as mentioned in Figure 3. The network is connected in parallel with the three legs/arms of the power switches IGBT, and the fourth wire (the neutral) is positioned between the two capacitors. The control block of this 3ph to 4W SAPF incorporates both SRF theory for reference current calculation and HCA for IGBT switches control. While HCA offers numerous advantages, it's important to highlight the issue of chattering, which can lead to variable switching frequencies. To tackle this concern, a PWM controller is integrated into the system to stabilize the switching frequency and reduce associated harmonic
losses. This paper outlines the design of a 3ph to 4W SAPF based on SRF, HCA, and PWM control, using both electrical and mathematical modeling.

The Active Power Filter (APF) demonstrates the capability to effectively address distortions stemming from both current and voltage, offering multidimensional flexibility, which makes it an appealing area for research. APFs are primarily employed for mitigating current distortions, including current harmonics, reactive power, and neutral current.

As depicted in Figure 3, the fundamental operation of the Shunt Active Power Filter (SAPF) involves supplying power from a three-line source to a non-linear load, with the SAPF connected at the Point of Common Coupling (PCC) to inject compensating current $i_{f_{(abc)}}$ into the PCC. This compensating current is generated by capturing the harmonic currents present in the load current $i_{L_{(abc)}}$ but phase-shifted by 180, effectively canceling out the harmonic current within the system. This process results in the source current $i_{S_{(abc)}}$ being free from harmonics. The current from the non-linear loads is sensed to determine the harmonic content, which is then used to calculate reference currents $i_{r_{(abc)}}*$ for controlling the switched Power Devices (denotes as $F_{(a,b,c)}$ and $\bar{F}_{(a,b,c)}$) of the SAPF.

4.1 Review of the SRF theory

One of the straightforward methods for generating reference currents is the time-domain-based Synchronous Reference Frame (SRF) method. In this approach, the three-phase load current in the a-b-c stationary frame is transformed into direct and quadrature-axis components. This transformation allows for the easy mitigation of harmonic components in the load current using a low-pass filter (LPF). The schematic diagram of the SRF method is depicted in Figure 15. The SRF method necessitates the use of a phase-locked loop (PLL) to provide the fundamental frequency for synchronization purposes. Additionally, this method requires a Proportional-Integral (PI) controller to maintain the DC link voltage at a constant level.

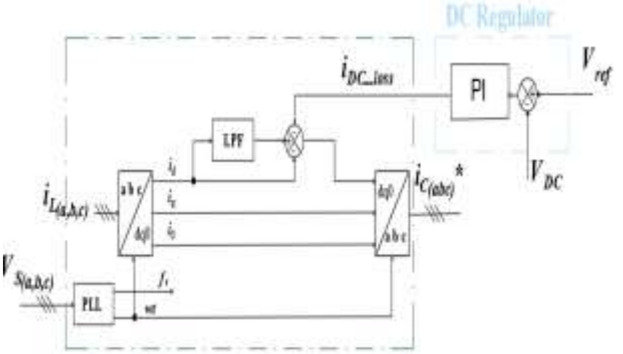

Fig. 15: Block diagram of the SRF theory

The load current in the a-b-c frame is transformed into 0-d-q frame components, a process described by equation 20:

$$\begin{pmatrix} i_d \\ i_q \\ i_0 \end{pmatrix} = \sqrt{\frac{2}{3}} \begin{pmatrix} \cos(\theta) & \cos(\theta - \frac{2\pi}{3}) & \cos(\theta + \frac{2\pi}{3}) \\ \sin(\theta) & \sin(\theta - \frac{2\pi}{3}) & \sin(\theta + \frac{2\pi}{3}) \\ \frac{1}{\sqrt{2}} & \frac{1}{\sqrt{2}} & \frac{1}{\sqrt{2}} \end{pmatrix} \begin{pmatrix} i_a \\ i_b \\ i_c \end{pmatrix} \quad (21)$$

The direct and quadrature axis components comprise both a DC component and multiple AC components, with the AC component referred to as the harmonic component. This harmonic component can be effectively filtered out using a Low-Pass Filter (LPF), while the steady-state error of each harmonic component is mitigated through the use of a Proportional-Integral (PI) controller.

$$\begin{cases} I_d = \bar{I}_d + \tilde{I}_d \\ I_q = I_q \end{cases} \quad (22)$$

Following the removal of the harmonic component from the direct and quadrature axis components, the 0-d-q frame components are transformed back into the a-b-c frame to derive the reference compensating current as presented in the equation (22).

$$i_{C(a,b,c)}* = \begin{pmatrix} i_{C_a}* \\ i_{C_b}* \\ i_{C_c}* \end{pmatrix} = \sqrt{\frac{2}{3}} \begin{pmatrix} \cos(\theta) & \cos(\theta) & \frac{1}{\sqrt{2}} \\ \cos(\theta - \frac{2\pi}{3}) & \sin(\theta - \frac{2\pi}{3}) & \frac{1}{\sqrt{2}} \\ \cos(\theta + \frac{2\pi}{3}) & \cos(\theta + \frac{2\pi}{3}) & \frac{1}{\sqrt{2}} \end{pmatrix} \begin{pmatrix} i_d \\ i_q \\ i_0 \end{pmatrix} \quad (23)$$

4.2 Review of the PWM VSI Controller

The principle of MLI control is illustrated in Figure 16. In this case, the difference (the error) between the reference current $i_{r_{(abc)}}*$ and the actual current $i_{f_{(abc)}}$ are applied to the controller input. The output signal of a controller (called a
modulator) is then compared to a triangular fixed frequency (carrier) signal to determine the switching sequence of the switches $F_{(a,b,c)}$ and $\bar{F}_{(a,b,c)}$. Therefore, the frequency of the triangular carrier sets the switching frequency of the VSI.

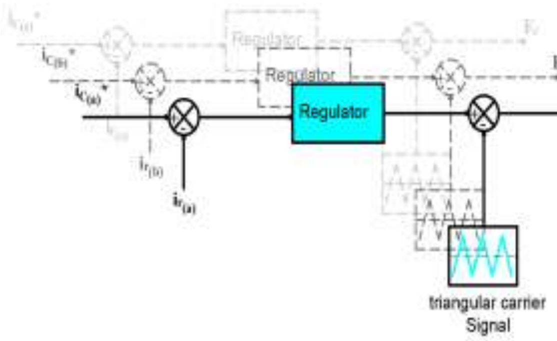

Fig. 16: Block diagram of the PWM controller

5 Simulation Results

We model and simulate the block diagram of the equivalent model of PV generator system with the SAPF under Matlab/Simulink software. The non-linear load contains 75 General Electric lamps model distributed over 3 AC phases (25 lamps in parallel for each phase). This load is powered up with the PV generator from the Softech 1STH-215P panel model. Also, a 3-phase SAPF is modeled to compensate harmonic generated by the nonlinear load. The main characteristics of the proposed system are illustrated in Table 2.

Table 2. PVG and SAPF System Parameters.

Parameters	***Value***
Source Voltage and frequency (V_S, F_S)	*230 V, 50 Hz*
Filter inductance (R_f, L_f)	*1 mΩ, 0.1 µH*
DC Link Capacitor (C_1, C_2)	*2200 µF*
Reference voltage V_{ref}	*600 V*

Figure 17 illustrates the different variations in irradiance, and the Maximum Power Point Tracking (MPPT) based on the Perturb and Observe (P&O) method promptly tracks the prospective maximum power point within a short duration. The P&O MPPT algorithm exhibits robustness against rapid changes in atmospheric conditions, resulting in minimal oscillations around the Maximum Power

Point (MPP) and achieving high efficiency of up to 92%.

Figure 18 and Figure 19 display the output voltage of the Photovoltaic Generator (PVG), while in Figure 20, we present the DC-link voltage across the capacitor, which is kept almost constant during changes in irradiance, with a drop in voltage lower than 25 V; the recovery time is about 0.02 s. Thus, this result confirms the efficiency of the DC-link voltage control system.

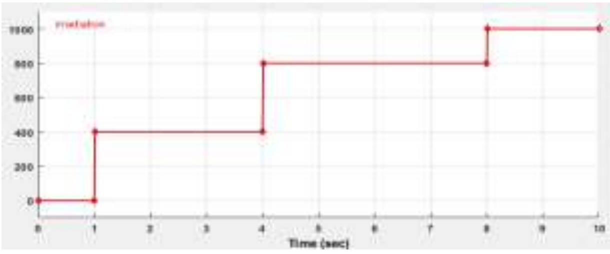

Fig. 17: Variation of Irradiance (Irr (W/m2))

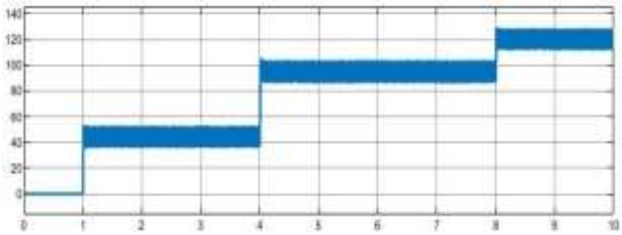

Fig. 18: PV array output currents (IPV (A))

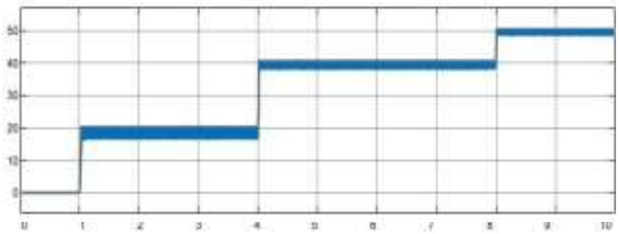

Fig. 19: PV array output voltage (VPV (V))

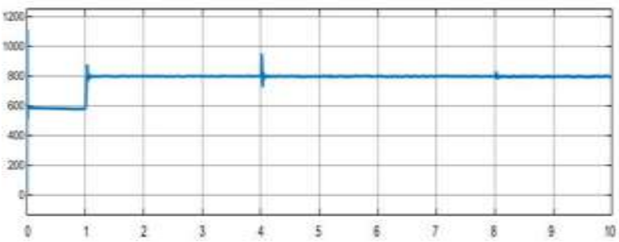

Fig. 20: dc-bus voltage (Vdc (V))

The AC output of this system is connected to a highly non-linear load, which injects harmonic current and reactive power into the main grid. An active power filter (APF) is implemented in parallel with the load. The APF addresses two main issues. Firstly, it aims to ensure that the current supplied to the mains system remains sinusoidal and reduces the harmonics generated by nonlinear loads. Secondly, the APF can perform additional tasks, such as boosting the power factor to unity and converting the current into an active component.

A PV-connected-to-grid system with an APF based on a three-legged, two-stage Voltage Source Inverter (VSI) with a midpoint 2C capacitor topology was developed and simulated using Simulink/MATLAB. The main parameters used in this paper are illustrated in Table 2.

The APF was connected in parallel at the Point of Common Coupling (PCC) with a three-phase four-wire nonlinear load, consisting of 75 new General Electric model Compact Fluorescent Lamps (CFLs) distributed across three AC phases, with 25 lamps in parallel for each phase. The model of those lamps was already presented in [22]. The fourth wire (the neutral) of the electrical power system was connected in the middle of the two capacitors.

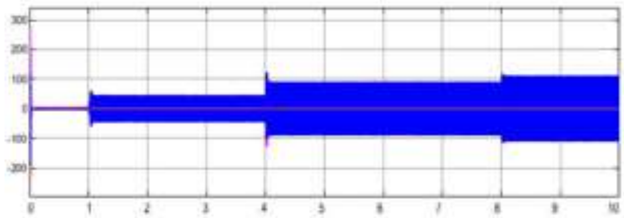

Fig. 21: The Source and the load Current waveforms Generated by the PV system

Furthermore, to investigate the effectiveness of the SAPF implemented in this work, a power device switch is enabled at t=0.02s to connect the Filter to the system. Figure 21 and Figure 22 present the source current waveforms before and after compensation. Also, Figure 23(a) and 23(b) and Figure 22 represent their FFT components before and after compensation.

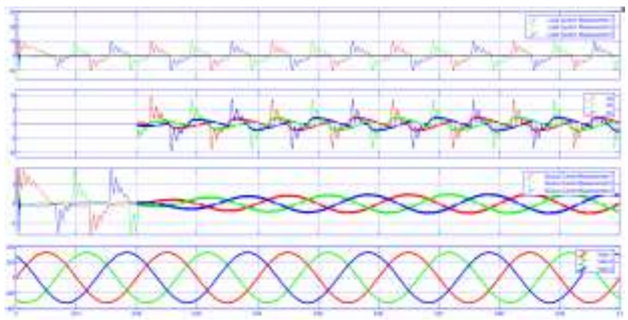

Fig. 22: The Source currents waveforms at different points before and after compensation

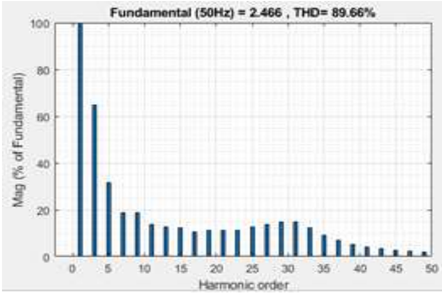

a)

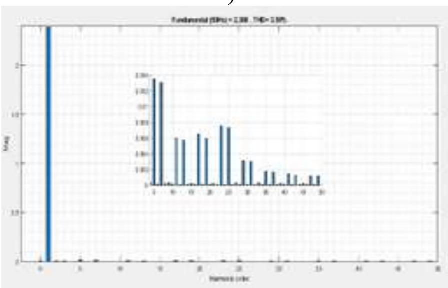

b)

Fig. 23: The FFT analysis of source current: a) without SAPF, b) with SAPF

The obtained results demonstrate a notable decrease in the Total Harmonic Distortion (THD) for both the source currents after compensation, resulting in the load voltage waveform becoming sinusoidal. The THD of the source current is greatly improved from 89.6% to 3.2%. Also, it can be noticed that the source current contains only the active component, which means that the reactive power is compensated, resulting in obtaining a good power factor (PF) close to 1. According to national and international standards, these results are within the allowed limits. This confirms that the algorithm mentioned in this paper has effectively compensated for harmonic currents by injecting equal yet opposite harmonic currents into the power network.

The Shunt Active Power Filter (SAPF) presented in this paper is specifically designed to address and compensate for harmonics, reactive power, and other disturbances introduced by nonlinear loads, thereby enhancing power factor and overall system performance.

Also, it shout be noted that the performance of the SAPF with other SAPF power circuit topologies will simulated and tested in this paper. Such as for the four-leg topology the founded THD is around 2.9% and for the three-half bridge (3H topology the THD is equal to 2.5% which attest the good implementation and the good performance of the three studied SAPF topologies.

In this section, we assess the applicability and effectiveness of the proposed SAPF. Despite the numerous advantages of the SAPF, it's worth noting that the DC bus of this filter utilizes a three-phase rectifier to supply power energy to the two midpoint capacitors, which are essential for compensating the reactive power generated by nonlinear loads. However, this approach can potentially introduce additional harmonic issues, particularly when dealing with highly nonlinear loads. To mitigate this challenge, we propose considering another power source for the midpoint capacitors based on PV or a wind system in future research endeavors. Additionally, we consider combining shunt and series active power filters to provide a more comprehensive solution for handling power quality issues associated with nonlinear loads.

6 Conclusion

It appears that you have provided a concise description of a paper or research project discussing the development of a three-phase, four-wire Shunt Active Power Filter (SAPF) designed to compensate for harmonics generated by nonlinear loads, specifically Compact Fluorescent Lamps (CFLs). The SAPF is integrated with a Photovoltaic (PV) system, and the primary objective of this system seems to be the maintenance of high-quality current and voltage in the electrical grid.

In summary, the key points highlighted in this description are as follows:

Shunt Active Power Filter (SAPF): A technology employed to mitigate harmonics and enhance power quality in electrical systems.

Nonlinear Load: In this context, it refers to devices like Compact Fluorescent Lamps (CFLs) that can introduce harmonics into the electrical grid due to their non-linear behavior.

PV System: A photovoltaic system likely generating electricity from solar panels.

High-Quality Power: The combined SAPF and PV system aims to ensure that the current and voltage supplied to the electrical grid meet high-quality standards, likely achieved by reducing harmonics and other disturbances.

References:

[1] A. Bertin, Canale. L, Ben Abdellah O, “Life Cycle Assessment of Lighting Systems and Light Loss Factor: A Case Study for Indoor Workplaces in France”, *Electronics*, 8, 1278, 2019.

[2] Fahad, A.-H.; Reza, M.-S. Single-Phase Shunt Active Power Filter Using Parabolic PWM for Current Control. *IEEE SEGE*, Oshawa, ON, Canada, 2019, 134-138.

[3] L. L. d. Souza, N, Rocha. D-A Fernandes. R-P-R de Sousa. And C-B, Jacobina. “Grid Harmonic Current Correction Based on Parallel Three-Phase Shunt Active Power Filter,” in *IEEE Transactions on Power Electronics*, 37, 2,1422-1434, 2022.

[4] Chihab, A.-Ait.; Ouadi H. Adaptive non-linear control of three-phase four-wire Shunt active power filters for unbalanced and nonlinear loads. *IFAC Proceedings,* 2014, 47, 3, 5061-5066.

[5] Chebabhi, A.; Fellah, M.-K. Comparative study of reference currents and DC bus voltage control for Three- Phase Four-Wire Four-Leg SAPF to compensate harmonics and reactive power with 3D SVM., *ISA Transactions*, 2015, 57, 360-372.

[6] Deffaf B.; Benbouhenni, H. Synergetic control for three-level voltage source inverter-based shunt active power filter to improve power quality. *Energy Reports*, 2023, 10, 1013-1027.

[7] Hekss, Z.; Abouloifa, A. Nonlinear adaptive control design with average performance analysis for a photovoltaic system based on half bridge shunt active power filter, *IJEPES 2021*, 125.

[8] Reddy, N.-B.; Pandian, A.; Chandra, O.; Ramamoorty, M. Performance and dynamic analysis of single switch AC-DC buck-boost buck converter. *IJITEE*, 8 4, 307- 313.

[9] Zinelaabidine, N., Karim, M., Bossoufi, B., & Taoussi, M. (2017, May). MPPT algorithm control for grid connected PV module. *In 2017 International Conference on Advanced Technologies for Signal and Image Processing (ATSIP)*, pp. 1-6, IEEE.

[10] Fabricio, E.-L-L.; Jacobina C. B.; Carlos, G.-A.-A.; Correa, M.-B.-R. Four H-bridge based shunt active power filter for three-phase four-wire system,” *IEEE APEC 2016*, Long Beach, CA, USA, 3641-3647.

[11] Keerthi, N.; Pandian, A.; Dhanasekaran, R. A Comprehensive Study on Shunt Active Power Filters for Grid – Tied wind systems. IOP Conf. Ser.: Mater. Sci. Eng. 993 012085. DOI: 10.1088/1757-899X/993/1/012085.

[12] Surgevil, T.; Akpinar, E. Application of shunt active power filter to isolated synchronous generator system. *2009 35th Annual Conference of IEEE IECON*, Porto, Portugal, 249-254.

[13] Lin, H.-C. Inter-Harmonic Identification Using Group-Harmonic Weighting Approach Based on the FFT,” in *IEEE TPEL 2008*, 23, 3, 1309-1319.

[14] Lin, H.-C. Inter-Harmonic Identification Using Group-Harmonic Weighting Approach Based on the FFT,” in *IEEE TPEL 2008*, 23, 3, 1309-1319.

[15] Boopathi, A.; Indragandhi, V. Comparative analysis of control techniques using a PV-based SAPF integrated grid system to enhance power quality, *J. Prime,* 2023, 5.

[16] Naftahi, K.; Abouloifa, A. Three-Phase Four-Wire Shunt Active Power Filter Based on the Hybrid Automaton Control with Instantaneous Reactive Power Theory. *IFAC-Papers* Online, 2022, 55, 12, 532-537.

[17] Sundaram, E.; Venugopal, M. On design and implementation of a phase three level shunt active power filter for harmonic reduction using synchronous reference frame theory. *IJEPES 2016*, 81, 40-47.

[18] Hanna Nohra, A.-F.; Kanaan, H.-Y.; M. Fadel. Comparative evaluation of current reference extraction methods for single-phase shunt active power filters. IECON 2016 - *42nd Annual Conference of the IEEE Industrial Electronics Society*, Florence, Italy, 3685-36901.

[19] Morales, J.; de Vicuna, L.-G.; Guzman, R.; Castilla, M.; Miret, J. Modeling and Sliding Mode Control for Three-Phase Active Power Filters Using the Vector Operation Technique. in *IEEE TIE 2018*, 65, 9, 6828- 6838.

[20] Antoniewicz, K.; Jasinski, M. Experimental comparison of hysteresis-based control and finite control state set Model Predictive Control of Shunt Active Power Filter. *WZEE 2015*, Kielce, Poland,1-6.

[21] Mohamed, H.; Mohamed, N.; Lassaad, S. Experimental Investigations of a CFLs Currents Harmonics Injection into an Electrical Network Grid. *ISAECT 2021*, 01-05.

[22] Pant, S., & Saini, R. P. (2019, November). Comparative study of MPPT techniques for solar photovoltaic system. *In 2019 International Conference on Electrical, Electronics and Computer Engineering (UPCON),* pp. 1-6. IEEE.

[23] Djamila Rekioua, T. R. (2015). Control of a Grid-Connected Photovoltaic System. *4th International Conference on Renewable Energy Research and Applications*. Palermo, Italy.

[24] F. Ansari, A. K. Jha, Maximum power point tracking using perturbation and observation as

well as incremental conductance algorithm, *International Journal of Research in Engineering & Applied Sciences, IJREAS*, Vol. 1, Issue 4 (December 2011).

[25] Bouselham, L., Hajji, B., & Hajji, H. (2015, December). Comparative study of different MPPT methods for photovoltaic system. *In 2015 3rd International Renewable and Sustainable Energy Conference (IRSEC)*, pp. 1-5. IEEE.

[26] Unal Yilmaza, A. K. (2018). PV system fuzzy logic MPPT method and PI control as a charge controller, *Renewable and Sustainable Energy Reviews*, Vol. 81, Part 1, January 2018, pp.994-1001.

[27] William Christopher, D. 1. (2013). Comparative Study of P&O and InC MPPT Algorithms. *American Journal of Engineering Research (AJER)*, Vol.02, Issue-12 402-408.

[28] Eseosa, O., & Kingsley, I. (2020). Comparative study of MPPT techniques for photovoltaic systems. Saudi *Journal of Engineering and Technology*, 5, 12-14.

Contribution of Individual Authors to the Creation of a Scientific Article (Ghostwriting Policy)

The authors equally contributed to the present research, at all stages from the formulation of the problem to the final findings and solution.

Sources of Funding for Research Presented in a Scientific Article or Scientific Article Itself

No funding was received for conducting this study.

Conflict of Interest

The authors have no conflicts of interest to declare.